2016-04-03

Evaluation of cytotoxicity profile and intracellular localisation of doxorubicin-loaded chitosan nanoparticles

Gabriele Dadalt Souto
Technological University Dublin

Zeineb Farhane
Technological University Dublin

Esen Efeoglu
Technological University Dublin

Alan Casey
Technological University Dublin, alan.casey@tudublin.ie

Jennifer McIntyre
Technological University Dublin

See next page for additional authors

Recommended Citation

"Evaluation of cytotoxicity profile and intracellular localisation of doxorubicin-loaded chitosan nanoparticles", Gabriele Dadalt Souto, Zeineb Farhane,Alan Casey, Esen Efeoglu, Jennifer McIntyre, Hugh James Byrne, Analytical and Bioanalytical Chemistry, 408, 5443-5455 (2016)

Authors
Gabriele Dadalt Souto, Zeineb Farhane, Esen Efeoglu, Alan Casey, Jennifer McIntyre, and Hugh Byrne

Evaluation of cytotoxicity profile and intracellular localisation of doxorubicin-loaded chitosan nanoparticles

Gabriele Dadalt Souto[1,*]

Zeineb Farhane[1,2]

Alan Casey[1]

Esen Efeoglu[1,2]

Jennifer McIntyre[1]

Hugh James Byrne[1]

[1]FOCAS Research Institute, Dublin Institute of Technology, Kevin Street, Dublin 8, Ireland

[2]School of Physics, Dublin Institute of Technology, Kevin Street, Dublin 8, Ireland

[*]Corresponding author

Present address: Faculdade de Farmácia, Universidade do Rio Grande do Sul, Porto Alegre RS, 90610-000, Brazil

Phone number: +555133085215

E-mail: gabrieledadalt@gmail.com

Funding

GDS was funded by the Brazilian National Council for Scientific and Technological Development (CNPq), through the Science without BordersProgram grant #236817/2013-2. ZF, AC, EE, JMcI and HJB are supported by Science Foundation Ireland Principle Investigator Award 11/PI/1108.

Abstract

In the emerging field of nanomedicine, targeted delivery of nanoparticle encapsulated active pharmaceutical ingredients (API) is seen as a potential significant development, promising improved pharmacokinetics and reduced side effects. In this context, understanding the cellular uptake of the nanoparticles and subsequent subcellular distribution of the API is of critical importance. Doxorubicin (DOX) was encapsulated within chitosan nanoparticles to investigate its intracellular delivery in A549 cells *in vitro*. Unloaded (CS-TPP) and doxorubicin-loaded (DOX-CS-TPP) chitosan nanoparticles were characterised for size (473±41 nm), polydispersity index (0.3±0.2), zeta potential (34±4 mV), drug content (76±7 μM) and encapsulation efficiency (95±1%). The cytotoxic response to DOX-CS-TPP was substantially stronger than to CS-TPP, although weaker than that of the equivalent free DOX. Fluorescence microscopy showed a dissimilar pattern of distribution of DOX within the cell, being predominantly localised in the nucleus for free form and in cytoplasm for DOX-CS-TPP. Confocal microscopy demonstrated endosomal localisation of DOX-CS-TPP. Numerical simulations, based on a rate equation model to describe the uptake and distribution of the free DOX, nanoparticles and DOX loaded nanoparticles within the cells, and the subsequent dose and time dependent cytotoxic responses, were used to further elucidate the API distribution processes. The study demonstrates that encapsulation of the API in nanoparticles results in a delayed release of the drug to the cell, resulting in a delayed cellular response. This work further demonstrates the potential of mathematical modelling in combination with intracellular imaging techniques to visualise and further understand the intracellular mechanisms of action of external agents, both APIs and nanoparticles in cells.

Keywords: nanomedicine, doxorubicin, chitosan nanoparticles, *in vitro* cytotoxicity, numerical simulations.

Introduction

Encapsulation of active pharmaceutical ingredients (API) in nanoparticle delivery vehicles potentially enables: targeting of specific tissues or cells, release of the API in a controlled manner, and/or reduction of the necessary dose, thereby reducing potential side effects (e.g. toxicity) of the treatment [1,2]. The greater specific surface area of nanoparticles, due to reduced size, enables greater biological activity and reactivity, when compared to larger particles [3], and therefore the biocompatibility of the nanocarriers themselves must be assured and adequate toxicity studies must be performed, *in vitro* and *in vivo*. Furthermore, it is important to study the nanoparticle uptake and trafficking mechanisms as well as the drug release at cellular and subcellular level. In this context, the *in vitro* study using model loaded nanoparticle drug systems, and kinetic modelling of response can add much to the understanding of the drug delivery processes.

Doxorubicin (DOX) is one of the most used chemotherapeutic agents for cancer treatment [4]. Nevertheless, problems related to resistance development [5], acute cardiotoxicity [6], low penetration and limited distribution in solid tumours [7], have led to investigations of alternative forms of administration. The majority of research has involved the association of doxorubicin to liposomes, exploring the interactions between lipid and drug charges [8]. However, indications of dermal and renal toxicity have been observed [9,10]. An alternative approach is to encapsulate doxorubicin within a positively charged nanocarrier, which would favour cellular adhesion and uptake, as cell membranes are negatively charged [11].

Chitosan (CS) is a linear cationic polysaccharide prepared through N-deacetylation of chitin. Generally recognised as safe, it has demonstrated biocompatible, non immunogenic, non toxic and biodegradable properties, and is thus a good candidate for pharmaceutical and biomedical applications [12,13]. In addition, considering intravenous administration, positively charged particles would interact with different blood components, which can favour different patterns of organ biodistribution and/or accumulation [14]. Chitosan nanoparticles can be formulated through several techniques, such as coacervation, co-precipitation, solvent evaporation, ionotropic gelation, and microemulsion, among others [11,15,16]. It should be noted that, although some regulatory definitions of nanoparticles restrict the term to a “particle with one or more dimensions of the order of 100 nm or less” [17], in other fields, such as Nanomedicine, the term is used to cover a broader size range and, for example, the International Standards Organisation Technical Committee on Nanotechnologies describes the “understanding and control of matter and processes at the nanoscale, typically, but not exclusively,

below 100 nanometers in one or more dimensions" [18] and it is in this context that the term nanoparticle is used in this work. Ionotropic gelation allows the preparation of chitosan nanoparticles in aqueous solution and avoids the use of organic solvents, high energy conditions and extreme conditions. Janes et al. [14], have employed ionic bridging with the dextran sulphate polyanion and polymer/drug (DOX) complexation to improve the drug delivery profile *in vitro*, and demonstrated intracellular distribution of the drug after the endocytosis of the loaded nanoparticles.

While the development of chitosan nanoparticles for administration of anticancer drugs and other substances is promising, the capacity to visualise the *in situ* behaviour of materials, particularly in the biological context, as well as characterise their interactions and toxicological effects, is of fundamental importance [19]. European Union directives [20] concerning substitution, reduction, and refinement of animal experimentation, prioritize the development of rapid and economically viable *in vitro* techniques for application in pharmaceutical and toxicological investigations. *In vitro* models are rapid, effective and usually well defined systems that can be used to evaluate several toxicological responses, establishing specific threshold of effects in cells and allowing studies of the structure-activity of nanomaterials [21]. Numerical simulations of nanoparticle uptake and cellular responses, based on rate equation models, have been demonstrated to extend the understanding which can be gleaned from conventional *in vitro* cytotoxicity assays, allowing a better conceptualisation of the underlying processes [22,23]. Thus, the aim of the present study was to investigate the intracellular delivery of the doxorubicin by loaded chitosan nanoparticles, as a model system, in an adenocarcinoma human alveolar basal epithelial cell line (A549) *in vitro*, through conventional cytotoxicity assays and fluorescence microscopy. The A549 cell line was chosen as clinical applications of DOX target solid tumors such as lung cancer, as well as for consistency with other studies [24-26, 41]. Adding to the study of Janes et al. [14], Numerical simulations of the toxic responses to the free drug, pristine and loaded nanoparticles are used to elucidate the underlying subcellular distribution and responses.

Materials and Methods

Materials

Chitosan hydrochloride (CL113, 110 kDa, 86% deacetylation degree) was purchased from Pronova Biopolymer (Norway). Doxorubicin hydrochloride (DOX, 98.0-102.0%), sodium tripolyphosphate (TPP, 85.0%) and sodium

dodecyl sulphate (SDS, ≥99.0%) were obtained from Sigma-Aldrich. Reagents for Alamar Blue® and 3-[4,5-dimethylthiazol-2-yl]-2,5-diphenyltetrazolium bromide (MTT) assays, as well as cell culture media and supplements and trypsin solution were purchased from Biosciences (Ireland). Ultrapure water used for all experiments was obtained from a Milli-Q water purification system (Millipore Co., USA).

Preparation of chitosan nanoparticles

Chitosan nanoparticles (CS-TPP) were prepared by ionotropic gelation [15]. Pre-formulation studies were performed to obtain chitosan nanoparticles with adequate amounts of each component, according to the methods described previously [14,16], with some modifications. Briefly, 21 mg of CS were dissolved in 10 mL of 1% acetic acid (pH 4.8 adjusted with 2M NaOH solution) and 500 µL of this solution were mixed with 10 µL of 10 mg/mL sodium dodecyl sulphate (SDS) and 10 µL of 10 mg/mL DOX solution (water was used for unloaded nanoparticles). 100 µL of a 2.9 mg/mL sodium tripolyphosphate (TPP) solution were added to the CS solution under magnetic stirring, leading to the immediate formation of the nanoparticles. The suspension formed was centrifuged at 1500 × *g* for 40 min for purification, the supernatant was discarded and the pellet re-suspended in water. The preparation process was performed inside a laminar flow hood. SDS was employed to counter-balance the charges in the particle and enable doxorubicin (pKa = 8.2) to be encapsulated.

Physicochemical characterisation of chitosan nanoparticles

Number mean diameter and particle size distribution were evaluated by dynamic light scattering and zeta potential was determined by laser Doppler microelectrophoresis (Zetasizer® Nano ZS, Malvern Instruments, UK). The system is routinely calibrated with NIST 3000 Series Nanosphere™ Size Standards, available from Thermo Scientific (60nm, 100nm and 1µm). Particle concentration was analysed by turbidimetry [27].

The method for quantification of DOX encapsulation in the DOX-CS-TPP nanoparticles used in this work was UV spectrophotometry (SpectraMax® M2, Molecular Devices, USA), as it is fast, precise and has good specificity [28].

Quantification of doxorubicin

Quantification of DOX was performed at 482 nm after validation of the analytical method by the determination of the following parameters: specificity, linearity, repeatability and accuracy. A standard solution of 10 mg/mL of DOX was used, from which calibration curves of absorbance at 482 nm were constructed over the DOX concentration range 34 – 311 µM (20 – 180 µg/mL). Encapsulation efficiency was calculated according to equation (S1), in which Total DOX is the absorbance of the suspensions of loaded nanoparticles before ultracentrifugation and Free DOX is the absorbance of the supernatant after ultracentrifugation of suspensions of loaded nanoparticles at 14000 × *g* for 10 min in centrifugal filter units (30K, Amicon®, EMD Millipore Co., MA, USA). The results are expressed as the mean of three different batches.

Equation (S1)

$$\text{DOX encapsulation efficiency} = \frac{\text{Total DOX} - \text{Free DOX}}{\text{Total DOX}}$$

Cell culture

The A549 human alveolar adenocarcinoma cell line was obtained from ATTC (Manassas, USA) and employed for cytotoxicity evaluations. Cells were cultured in Dulbecco's Modified Eagle's Medium (DMEM) F-12, supplemented with 10% foetal bovine serum (FBS), 45 UI/mL penicillin and 45 µg/mL streptomycin, and kept in humidified incubator at 37 °C (5% CO_2).

Cytotoxicity studies

Cells were seeded in 96-well plates at densities of 1×10^5, 7×10^4 and 3×10^4 cells/mL for 24, 48 and 72h of exposure, respectively. Cells were allowed to attach for 24h and then washed with phosphate buffered saline (PBS) prior to treatment with fresh medium containing unloaded chitosan nanoparticles (CS-TPP), solutions of doxorubicin in water (free DOX) or doxorubicin-loaded chitosan nanoparticles (DOX-CS-TPP) in the concentration range 1.5×10^{-4} – 7.6 µM (8.8×10^{-5} – 4.4 µg/mL) of DOX. CS-TPP results are expressed in particles/mL (1×10^7 – 5×10^{11} particles/mL, as calculated by turbidimetry). After the requisite exposure time, cell viability was measured by MTT and AB assays in accordance with manufacturer's instructions.

Live cell imaging

Fluorescence microscopy

A549 cells were seeded in glass bottom Petri dishes at a density of 1×10^4 cells/dish in DMEM F-12 medium supplemented with 10% FBS, and kept in a humidified incubator at 37 °C (5% CO_2). Cells were allowed to attach for 24h, washed with PBS and exposed to 7.6 µM (4.4 µg/mL) of free DOX or 5×10^{11} particles/mL of CS-TPP and DOX-CS-TPP (as calculated by turbidimetry) or fresh medium as a negative control, and incubated for 24h. After the requisite exposure time, cells were washed three times with pre-warmed PBS (37 °C). Hoechst 33342 stain solution (initial concentration of 20 mM), used for DNA and nucleus staining of eukaryotic cells, was diluted 2000 times in PBS and cells were stained for 10 min. Before imaging, cells were washed three times with PBS to assure complete removal of non-internalised stain. Images were obtained through the software AxioVision (version 4.8.1.0, Carl Zeiss Imaging Solutions Gmbh, Germany), annexed to an inverted microscope for transmitted light and epifluorescence Axiovert 200M (Carl Zeiss, Germany), equipped with AxioCamHR camera. Brightfield settings with 63x objective, as well as DAPI (blue) and DsRed (red) filters were used for imaging.

Confocal microscopy

A549 cells were seeded in glass bottom Petri dishes at a density of 1×10^4 cells/dish in DMEM F-12 medium supplemented with 10% FBS, and kept in a humidified incubator at 37 °C (5% CO_2). Cells were allowed to attach for 24h, washed with PBS and subjected to early endosomal staining (Cell Light Early Endosomes-RFP, BacMam 2.0, 30 ppc) for 16h. After this period, cells were exposed to 7.6 µM (4.4 µg/mL) of free DOX or 5×10^{11} particles/mL of CS-TPP and DOX-CS-TPP (as calculated by turbidimetry) or fresh medium as negative control, and incubated for 4h. After exposure for the appropriate time, cells were washed three times with pre-warmed PBS (37 °C), to ensure complete removal of non-internalised stain. Images were obtained through confocal fluorescence microscope LSM 510 META (version 3.2 SP2, Carl Zeiss, Germany), using fixed excitation wavelength at 488 nm and fluorescence detection was achieved with a 505-530 nm band pass filter (green) and a 585 nm long pass filter (red).

Statistical analyses

All experiments were carried out in triplicate (three independent experiments). MTT and AB assays results are expressed as mean percentage relative to unexposed control ± standard deviation (SD), wherein unexposed control values were considered 100%. Differences among groups were statistically analysed through the software GraphPad Prism (version 5.0, GraphPad Software, Inc., USA), and a p-value < 0.05 was considered significant. Data normality was confirmed by the Kolmogorov-Smirnov test and the homogeneity of variances was evaluated using the Bartlett test. One-way ANOVA followed by Bonferroni's post-test was employed for data with normal distribution and homogeneous variances. Non-parametric Kruskal-Wallis test followed by Dunn's post-test was applied to samples without normal distribution and/or inhomogeneous variances. Cytotoxicity data were adjusted to a sigmoidal curve through the software SigmaPlot™ (version 10.0, Systat Software, Inc., USA) and a four-parameter model (Eq. 1) was used to calculate the effective nanomaterial concentration that caused 50% of the maximum observed inhibition compared to unexposed controls (EC_{50}).

Equation (1)
$$y = \min + \frac{\max - \min}{1+(\frac{x}{EC50})^{Hillslope}}$$

Numerical simulations were performed by integration using the iterative Euler approach [29] and SigmaPlot™ (v.10.0) was used to generate the values and graphs.

Results

Preparation and physicochemical characterisation of chitosan nanoparticles

The characterisation results for size distribution, surface charge and particle concentration of chitosan nanoparticle suspensions are listed in Table 1. The number size distribution of unloaded (CS-TPP) and doxorubicin-loaded (DOX-CS-TPP) nanoparticles is illustrated in Online Resource 1 (Figure S1).
In order to quantify the encapsulation of DOX, calibration curves were constructed by plotting absorbance versus DOX concentration over the range 34 – 311 µM. The least squares method was applied for linear regression analysis and the calculated value for the correlation coefficient (r^2 = 0.9996) showed excellent linearity of the calibration curve, with no significant deviation from linearity. The specificity was determined by the absorption spectrum of CS-TPP formulations, in comparison with the absorption spectra of free DOX and DOX added to CS-TPP (Online Resource 1, Figure S2). The absorbance of CS-TPP was determined to be 0.0128 at 482 nm, thus achieving good selectivity towards DOX, without any potential interference from the formulation.

Repeatability (inter-day precision) was studied by calculating the relative standard deviation (RSD) for three independent determinations of three different concentrations, from which a value of RSD < 5% was obtained. In addition, the accuracy of the analytical method, which is the closeness of the test results obtained by the method to the true value, was calculated by three replicate determinations of concentrations of 34, 145 and 256 μM in the presence of CS-TPP. The results showed that the proposed method has an accuracy of 103.9 ± 2.0% within the desired range.

In this way, the DOX concentration in DOX-CS-TPP formulations was determined to be 76 ± 7 μM by direct absorbance determination, and the encapsulation efficiency after purification was 95 ± 1%, according to absorbance determination of the supernatant. Thus, a DOX-CS-TPP concentration of 1 particle/mL corresponds to a dose of $8.29 \pm 0.92 \times 10^{-12}$ μM.

Cytotoxicity studies

Figure 1 illustrates the dose dependent cytotoxic responses for both MTT and AB at 24, 48 and 72h. For both assays, a significant dose dependent response is observed, the loss of viability increasing with increasing dose and exposure time. Notably, the MTT is somewhat more responsive to the DOX exposure, particularly at shorter exposure times. For the case of CS-TPP nanoparticles, a significant toxic response is also observed (40.6 ± 4.2% and 77.0 ± 9.0% viability, MTT and AB respectively, at 5×10^{11} particles/mL at 48h), although for equivalent exposure times, the response for both assays is considerably lower over the exposure range, compared to the free DOX exposure range (Figure 1A and B). As is the case for free DOX, MTT is seen to be a more sensitive assay than AB (Figure 1C and D) (EC_{50} of 0.38 ± 0.08 and 0.93 ± 0.29 μM of DOX for MTT and AB, respectively, at 24h). When exposed to DOX loaded chitosan nanoparticles, DOX-CS-TPP (Figure 1E and F), over the same nanoparticle exposure dose range, a stronger toxic response (difference Max – Min viability of 111.8 and 109.7 for MTT and AB, respectively, at 72h) is elicited than for unloaded CS-TPP nanoparticles (difference Max – Min viability of 64.2 and 10.8 for MTT and AB, respectively, at 72h), indicating some degree of success in the intracellular delivery of the chemotherapeutic agent encapsulated as cargo in the nano drug delivery vehicle. Over the same equivalent DOX dose range, however, the toxic response appears weaker, at least at the shorter exposure time of 24h (at the higher dose, DOX elicits 35.0 ± 14.4% and 55.8 ± 16.3% viability, while DOX-CS-TPP elicits 48.1 ± 6.6% and 81.6 ± 6.0% viability, for MTT and AB, respectively), indicating a reduced intracellular rate of delivery of DOX.

The lines of Figure 1 show fits of equation 1 to the respective experimental data. The associated fit parameters are tabulated in Table S1 (Online Resource 1). In general, a trend of decreasing EC_{50} with increasing exposure time reflects the increasing toxic response, and the relatively lower values for MTT compared to AB for each exposure time reflects the higher sensitivity of that assay. Of particular relevance is the comparison of the EC_{50} values for free DOX exposure compared to the equivalent DOX values for the DOX-CS-TPP exposures, which, for both MTT and AB, reveal a considerably higher EC_{50} dose equivalent for the latter (AB EC_{50} of 0.26 ± 0.06 and 0.07 ± 0.02 μM of DOX for DOX-CS-TPP and free DOX, respectively, at 72h).

Live cell imaging

Firstly, cells were observed using fluorescent microscopy, after incubation for 24h with test suspensions and the Hoechst 33342 blue stain for the nucleus. Red fluorescence imaging was used to visualize DOX. Figure 2 shows that the red fluorescence in the cells exposed to free DOX is concentrated in the nucleus. In comparison, cells exposed to DOX-CS-TPP show less co-localization of the red fluorescence with the nuclear stain.

Subsequently, A549 cells were incubated for 4h with CS-TPP, free DOX or DOX-CS-TPP to further investigate the cellular uptake behavior by confocal laser scanning microscopy (CLSM), after early endosomal staining. As shown in Figure 3, the green fluorescence of the endosomal stain was observed in all the cells, independent of the treatment, showing successful staining of early endosomes. After exposure to unloaded CS-TPP nanoparticles, the endosomal staining is concentrated in small vesicles, distributed throughout the cytoplasm, consistent with uptake of the nanoparticles into early endosomes [30]. Furthermore, the intracellular DOX can be identified by the red fluorescence, which is observed predominantly in the nuclei for free DOX treated cells. For DOX-CS-TPP treated cells, DOX fluorescence is also present in the cytoplasm, corroborating the fluorescence microscopy images, and indicates its localization in early endosomes (yellowish color), as well as in other subcellular compartments.

Numerical simulations using rate equation model

The cellular uptake of, and responses to, the external agents can be numerically simulated in order to further elucidate the different responses. Such an approach, based on a rate equation model, has previously been

employed to simulate the time and dose dependent cytotoxicity of polymeric dendrimer nanoparticles, as well as the observed differences in responses for different cytotoxic assays and cell lines [23,31].

In a similar fashion, for a dose D, the uptake of DOX within the cells can be described by the first order rate equation:

Equation (2) $$\frac{dN_{DOX}}{dt} = k_{DOX}(D - N_{DOX})$$

where N_{DOX} is the dose of internalised DOX and k_{DOX} is the rate of internalisation. The term ($D-N_{DOX}$) allows for depletion of the applied dose by the uptake process. The accepted mode of action of DOX, once internalised, is the rapid localisation in the nucleus, in which it intercalates with DNA, resulting in the onset of apoptosis [32]. In the formalism of Black and Leff [33], the DOX binds with receptors, according to the equation:

Equation (3) $$\frac{dN_{RB}}{dt} = k_{RB}N_{DOX}(N_{Rmax} - N_{RB})$$

where N_{RB} is the number of bound receptors, k_{RB} is the receptor binding rate, and N_{Rmax} is the maximum number of available receptors. The MTT assay reveals changes in mitochondrial activity, which, as a result of the action of DOX in the nucleus and the onset of apoptosis, can be modelled according to:

Equation (4) $$\frac{dMTT}{dt} = MTT_{max} - k_{MTT}MTT.N_{RB}$$

where MTT is the response of the assay as a function of time, MTT_{max} being the maximum at zero exposure, and k_{MTT} is the rate of response of the mitochondria as a result of the nuclear insult of DOX.

Equations (2-4) can be solved numerically, generating a time dependence of the cellular uptake of and response to DOX exposure, over the dose range. Figures 4A and B show the simulated dose dependent response for the time points of 24, 48 and 72 hrs, as compared to the experimentally determined responses of Figure 1. A list of fit parameters is provided in the Online Resource 1. As shown in Figure 4C, for 0.1 μM dose, a rapid uptake of DOX and binding to the nuclear receptors is followed by a slower response of the mitochondrial activity. The dose dependent responses at the experimentally measured time points are well reproduced by the simulation based on the rate equation model.

For the case of the AB response, the experimental results are not well simulated by either a cascade of AB response, triggered by the MTT response of Equation 4, or even the AB response triggered by the nuclear receptor binding described by Equation 3. Instead, the closest simulation of the experimental observations was achieved by providing an alternative route of intracellular interaction of the internalised DOX molecules. In addition to the mode of action of DNA intercalation, internalised DOX can also lead to the generation of free

radicals, resulting in DNA and cell membrane damage [34]. The response can be simulated such that, after uptake according to Equation 2, the DOX interacts according to:

Equation (5) $$\frac{dN_{FR}}{dt} = k_{FR} N_{DOX}^{0.5} (N_{FRmax} - N_{FR})$$

where N_{FR} is the number of generated free radicals, k_{FR} is the radical generation rate, and N_{FRmax} is the maximum number of free radicals which can be generated. The square root dependence on N_{DOX} is indicative of a cascade process of one DOX molecule resulting in two or more radicals. The AB assay registers changes in cytoplasmic activity, which, as a result of the action of DOX in the cytoplasm, can be modelled according to:

Equation (6) $$\frac{dAB}{dt} = AB_{max} - k_{AB} AB \,.\, N_{FR}$$

where AB is the response of the assay as a function of time, AB_{max} being the maximum at zero exposure, and k_{AB} is the rate of response of the cytoplasmic activity as a result of the insult of DOX. Figure 5B shows the simulated AB response to the DOX exposure, compared to the experimentally observed responses. As shown in Figure 4C, the AB response (at a dose of 0.1 μM) is slower than that of the MTT, resulting in lower cytotoxic responses at the respective time and dose points.

The uptake of, and cellular cytotoxic response to, CS-TPP nanoparticle exposure, as a function of time and dose, can similarly be simulated. For a dose D, the uptake of CS-TPP within the cells can be described by the first order rate equation:

Equation (7) $$\frac{dN_{NP}}{dt} = k_{NP}(D - N_{NP})$$

where N_{NP} is the dose of internalised CS-TPP nanoparticles and k_{NP} is the rate of internalisation. The term ($D-N_{NP}$) allows for depletion of the applied dose by the uptake process. As shown in Figure 3, using CLSM, the nanoparticles are endocytosed and the common mechanism of toxicity is further trafficking through lysosomes and the generation of oxidative stress, resulting in cell damage and apoptosis [35]. Following the approach of Maher et al. [23], the cellular response is the result of an interaction of the endocytosed nanoparticles with an intracellular source of reactive oxygen species (ROS), N_{source}, which is depleted by the ROS generation process. Thus,

Equation (8) $$\frac{dN_{Source}}{dt} = -k_A . N_{NP^A} . N_{Source}$$

where k_A is the interaction rate for the nanoparticles and source, and A is an empirical constant. The generation of ROS is then described by:

Equation (9) $$\frac{dN_{ROS}}{dt} = -k_A . N_{NP^A} . N_{Source} - k_q . N_{ROS} . N_{GSH}$$

The second term of Equation (9) describes the quenching of the ROS at a rate k_q, and depends on both; ROS levels, N_{ROS}, and antioxidant levels, N_{GSH} ($N_{GSH}(0) = 0$). In the study by Mukerjee and Byrne [31], the antioxidant levels were represented by the experimentally measured values of glutathione (GSH) which are represented by:

Equation (10) $$\frac{dN_{GSH}}{dt} = k_{GSH} - N_{ROS}(t).N_{GSH}(t).k_q$$

For both MTT and AB, the loss of viability is represented by equations (4) and (6), replacing N_{RB} or N_{FR} by N_{ROS} and nanoparticle specific rate constants k'_{MTT} and k'_{AB}. The resultant simulated plots of dose dependent viability for the time points of 24, 48 and 72 hrs are shown in Figure 5 (A) MTT, and (B) AB. The fit parameters are provided in the Online Resource 1. The simulations satisfactorily reproduce the trends observed experimentally. A notable difference between the simulations for DOX and CS-TPP is the rate of uptake of the respective agent by the cells, as shown in Figure 5C, which is substantially slower for the nanoparticles than for the molecular species, (k_{DOX}= 2 hr^{-1}, k_{NP} = 0.5 hr^{-1}) consistent with the observations of Salvati et al. [30] for polystyrene nanoparticles uptake compared to free organic fluorescent dye molecules.

To simulate the cytotoxic responses to the nanoparticle encapsulated DOX, the DOX-CS-TPP uptake was simulated according to Equation (7), and subsequent responses to the endocytosed nanoparticles were evaluated according to Equations (8-10), in all cases using the same fit parameters as for CS-TPP (Online Resource 1). As shown in Figure 3, however, once endocytosed, the DOX-CS-TPP release the DOX into the cytosol, from where it reaches the nucleus. The process is simulated according to the equation:

Equation (11) $$\frac{dN_{DOX}}{dt} = k_R . N_{NP}$$

where k_R denotes the rate of release of DOX from the endosomes. The value of k_R incorporates the scaling factor of the encapsulation efficiency. The released DOX can then interact with the cell, as described by Equations (3-6). In a simple approximation, the combined effect of the CS-TPP nanoparticles and the released DOX can be taken to be a linear combination, such that the viability of the cell, as measured by the MTT and AB assays, respectively, can be represented by:

Equation (12) $$\frac{dMTT}{dt} = MTT_{max} - k_{MTT}MTT.N_{RB} - k'_{MTT}MTT.N_{ROS}$$

Equation (13) $$\frac{dAB}{dt} = AB_{max} - k_{AB}AB.N_{FR} - k'_{AB}AB.N_{ROS}$$

For both MTT and AB, k and k' indicate the rates of the two independent routes towards cell death, elicited by the DOX and CS-TPP nanoparticles respectively. The simulations of Figure 6 provide a reasonable reproduction of the experimental observations for the MTT and AB responses at 24, 48 and 72 hrs, although deviations may

be an indication of a more complex release process of DOX from the CS-TPP nanoparticles, and subsequently from the endosomes, or a co-operative or even competing effect of the two toxicants.

Figure 7 provides a visualisation of the time dependence of the DOX-CS-TPP nanoparticle uptake and different cellular responses. It is clear that, for both MTT and AB, the loss of viability due to the toxic response to the nanoparticles is substantial (NP Response), although more significantly so for MTT than for AB. Notably, the DOX response, for both assays is delayed significantly compared to the response to the free DOX (Figure 4C), due to the delayed release of the API from the nanoparticles, encapsulated within the intracellular endosomes/lysosomes.

Discussion

In the present work, chitosan (CS) was ionically cross-linked with the counter-ion sodium tripolyphosphate (TPP) through ionotropic gelation, in which positive and negative groups of each component interact to form hydrogel nanoparticles [15]. The results show that, for both CS-TPP and DOX-CS-TPP nanoparticles, monomodal and nanometric distributions (220 – 1106 nm) were obtained. Zeta potential values demonstrate the positive characteristic of the particle surface charge, even in the presence of SDS. Furthermore, suspensions presented adequate polydispersity index and particle concentration for nanoscale formulations [27]. Besides, the overall results of the determination of validation parameters analysed demonstrated the adequacy of the proposed method for quantification of DOX [36].

The synthesized chitosan nanoparticles loaded with the API doxorubicin were used in this study to elucidate the cytotoxicity and internalization profiles in A549 cells. A variety of endpoints are commonly used to evaluate cytotoxic responses of cell lines *in vitro*. Each cytotoxicity assay measures a different response or adjacent cell function. The Alamar Blue® assay is based on fluorescence, which indicates the innate cellular metabolic activity by the conversion of resazurin (non fluorescent) in resorufin (fluorescent) [37], while the MTT assay indicates mainly mitochondrial metabolism [38]. The *in vitro* toxicity is expressed as the effective concentration for reduction of 50% of cell viability (EC_{50}), which is essentially the midway concentration between minimum and maximum responses. The EC_{50} values for A549 cells found in this work for free DOX are comparable with other studies [39-41], ranging from 0.5 to 5 μM. Notably, however, unless minimum and maximum responses are close for different test substances/formulations, EC_{50} values are difficult to compare among the variety of cell lines, assays employed and nanoparticle characteristics [22,23].

In order to further understand the differences in cytotoxic responses to the free API and the API loaded in the nanoparticles, it is necessary to image the localization of the drug within the cells. Live cell imaging was carried out following 4h or 24h exposure to CS-TPP, free DOX or DOX-CS-TPP, or fresh medium as negative control. The fluorescence microscopy observations indicate that DOX localizes in the nucleus to a greater extent when in free form compared to the DOX confined in nanoparticles, which may imply that the internalization process of nanoparticles, when compared to the free drug, occurs through a different and/or slower mechanism. However, due to limited resolution of this technique, it was not entirely clear whether the nanoparticles released DOX on the surface of the cells or whether they were internalized into the cells.

In this way, we performed confocal laser scanning microscopy (CLSM) in order to better visualize the DOX localization within the cells. Our results clearly indicate that DOX-CS-TPP nanoparticles are taken up by the cell mostly through endocytosis and DOX is released to the nucleus afterwards, in contrast to free DOX, which is transported into cells *via* passive diffusion [41,42] after which it is rapidly localized within the nucleus.

Different cell uptake mechanisms of free drugs and drug-loaded nanoparticles are widely described in scientific literature [43-45]. In particular, doxorubicin is useful for these studies due to its pronounced red fluorescence. It is hypothesized that the acidic environment of endosomal/lysosomal compartments helps the release of DOX from nanoparticles, reaching the nucleus thereafter [45]. The delayed release of DOX, reducing the overall cytotoxicity, might be beneficial depending on the ultimate effect in the cell. In order to elucidate these potentially different underlying subcellular responses, numerical simulations from cytotoxicity assays data were performed.

Numerical simulations, based on a rate equation model to describe the uptake and distribution of the free DOX, nanoparticles and DOX loaded nanoparticles within the cells, and the subsequent dose and time dependent cytotoxic responses, are used to further elucidate the API distribution processes. The study demonstrates that encapsulation of the API in nanoparticles results in a delayed release of the drug to the cell, resulting in a delayed cellular response. Moreover, unloaded nanoparticles also displayed a degree of toxicity that may indicate that DOX-CS-TPP cytotoxicity occurs through different cell death mechanisms, which in turn can potentiate the cellular responses. These have been independently modelled for the free DOX and pristine CS-TPP nanoparticles, and the mechanisms combined in the model for the DOX-CS-TPP toxic response for both assays. As discussed in the introduction, encapsulation of APIs in nanoparticle delivery vehicles has several potential advantages for clinical treatments: the passive targeting of specific tissues or cells, release of the API in a controlled manner, reduction of the necessary dose and/or number of administrations, thereby

reducing potential side effects, ultimately improving efficacy and patient compliance [2,46]. The cellular internalization of chitosan nanoparticles and the retention of encapsulated DOX bioactivity have been demonstrated [11,14]. However, no previous reports have investigated unloaded and DOX-loaded chitosan nanoparticles of approximately 500 nm in such depth. This study demonstrates that DOX encapsulated within chitosan nanoparticles, although they are engulfed in endosomal vesicles, remains bioavailable and elicits a toxic response in the cells, *in vitro*, in a similar fashion to the free API. Endoscytosis of the nanoparticles containing API results, however, in a delayed release of the drug to the cell, resulting in a delayed cellular response which could be potentially further controlled by tailoring the physicochemical properties of the nanoparticle.

In summary, unloaded and doxorubicin-loaded chitosan nanoparticles were successfully synthesized and physicochemically characterized for further use in *in vitro* experiments. This work sheds new light on the differences of cellular internalization of free or encapsulated APIs, the latter having a delayed response. Although free doxorubicin elicited a stronger response in comparison to doxorubicin-loaded chitosan nanoparticles, such a delayed release of the drug from the nanoparticles to the cell. This effect results in similar *in vitro* efficacy in the time frame of the cytotoxicity experiment, but may have different implications in an *in vivo* system. For example, it may overcome partially or completely the development of tumour resistance during chemotherapy, or it may show a better selectivity towards cancerous cells in comparison to non-cancerous cells. These hypotheses should be addressed in future studies. We further demonstrated the potential of mathematical modelling to visualise and better understand the intracellular mechanisms of action of external agents, both APIs and nanoparticles in cells. DOX itself is a well-known anticancer agent that triggers tumor resistance and cardiotoxicity during chemotherapy. Its selectivity towards carcinogenic and non-carcinogenic cells is low [39], however, and ultimately, improved selectivity of nanoformulations, potentially by adding additional cell targeting functionalities [47,48], should be demonstrated. DOX is usually administered intravenously, but nanoparticles can be administered intravenously or through the pulmonary route in liquid or powder form. Although, a full study of the metabolisation of DOX and of the stability of the nanoparticles, administered according to established clinical protocols is beyond the scope of the present work, comparative *in vitro*/*in vivo* studies must be conducted in order to fully demonstrate mathematical modelling as a viable alternative to the experimentally testing of nanoparticles.

Acknowledgements

This research was carried out under funding by the Brazilian National Council for Scientific and Technological Development (CNPq), through the Science without Borders Program grant #236817/2013-2, awarded to GDS. ZF, AC, EE, JMcI and HJB are supported by Science Foundation Ireland Principle Investigator Award 11/PI/1108.

Conflict of Interest

The authors declare that they have no conflict of interest.

References

1. Moghimi SM, Hunter AC, Murray JC. Nanomedicine: current status and future prospects. FASEB J. 2005;19:311-30.
2. Schütz CA, Juillerat-Jeanneret L, Mueller H, Lynch I, Riediker M. Therapeutic nanoparticles in clinics and under clinical evaluation. Nanomedicine-UK. 2013;8:449-67.
3. Oberdörster G, Oberdörster E, Oberdörster J. Nanotoxicology: an emerging discipline evolving from studies of ultrafine particles. Environ Health Persp. 2005;113:823-39.
4. Octavia Y, Tocchetti CG, Gabrielson KL, Janssens S, Crijns HJ, Moens AL. Doxorubicin-induced cardiomyopathy: from molecular mechanisms to therapeutic strategies. J Mol Cell Cardiol. 2012;52:1213-25.
5. Goldstein LJ, Galski H, Fojo A, Willingham M, Lai SL, Gazdar A, Pirker R, Green A, Crist W, Brodeur GM, Lieber M, Cossman J, Gottesman MM, Pastan I. Expression of multidrug resistance gene in human cancers. J Natl Cancer Inst. 1989;81:116-24.
6. Von Hoff D, Rozencweig M, Piccart M. The cardiotoxicity of anticancer agents, Semin Oncol. 1982;9:23-33.
7. Primeau AJ, Rendon A, Hedley D, Lilge L, Tannock IF. The distribution of the anticancer drug doxorubicin in relation to blood vessels in solid tumors. Clin Cancer Res. 2005;11:8782-8.
8. Hofheinz RD, Gnad-Vogt SU, Beyer U, Hochhaus A. Liposomal encapsulated anticancer drugs. Anticancer Drugs. 2005;16:691-707.

9. Manil L, Couvreur P, Mahieu P. Acute renal toxicity of doxorubicin (adriamycin)-loaded cyanoacrylate nanoparticles. Pharm Res. 1995;12:85-7.

10. Lorusso D, Di Stefano A, Carone V, Fagotti A, Pisconti S, Scambia G. Pegylated liposomal doxorubicin-related palmar-plantar erythrodysesthesia (‘hand-foot’ syndrome). Ann Oncol. 2007;18:1159-64.

11. Tan ML, Choong PFM, Dass CR. Review: doxorubicin delivery systems based on chitosan for cancer therapy. J Phar Pharmacol. 2009;61:131-42.

12. Siqueira NM, Contri RV, Paese K, Beck RCR, Pohlmann AR, Guterres SS. Innovative sunscreen formulation based on benzophenone-3-loaded chitosan-coated polymeric nanocapsules. Skin Pharmacol Physiol. 2011;24:166-74.

13. Nafee N, Schneider M, Schaefer UF, Lehr CM. Relevance of the colloidal stability of chitosan/PLGA nanoparticles on their cytotoxicity profile. Int J Pharm. 2009;381:130-9.

14. Janes KA, Fresneau MP, Marazuela A, Fabra A, Alonso MJ. Chitosan nanoparticles as delivery systems for doxorubicin. J Control Rel. 2001;73:255-67.

15. Sureshkumar MK, Das D, Mallia MB, Gupta PC. Adsorption of uranium from aqueous solution using chitosan-tripolyphosphate (CTPP) beads. J Haz Mat. 2010;184:65-72.

16. Bugnicourt L, Alcouffe P, Ladavière C. Elaboration of chitosan nanoparticles: Favorable impact of a mild thermal treatment to obtain finely divided, spherical, and colloidally stable objects. Col Surf A. 2014;457:476-86.

17. European Commission. Definition of Nanoparticle. In: Scientific Committees Toolbox. Scientific Committee on Emergent and Newly Identified Health Risks. 2007. http://ec.europa.eu/health/scientific_committees/opinions_layman/glossary/mno/nanoparticle.htm. Accessed 19 Apr 2016.

18. International Organisation for Standardization. In: Technical Committee 229 Nanotechnologies (ISO/TC 229). 2005. http://www.iso.org/iso/iso_technical_committee?commid=381983. Accessed 19 Apr 2016.

19. 17Keating M, Byrne HJ. Raman spectroscopy in nanomedicine: current status and future perspectives. Nanomedicine. 2013;8:1-17.

20. 18European Parliament and the Council of the European Union. Directive 2010/63/EU of the European Parliament and the Council of 22 September 2010 on the protection of animals used for scientific purposes. OJEU 2010, L 276/33.

21. 19Huang, Y.-W.; C-H, Wu.; Aronstam, R.S. Toxicity of transition metal oxide nanoparticles: Recent insights from in vitro studies. Materials v. 3, p. 4842–4859, 2010.
22. 20Mukherjee SP, Davoren M, Byrne HJ. In vitro mammalian cytotoxicological study of PAMAM dendrimers – towards quantitative structure activity relationships. Toxicol In Vitro. 2010;24:169-77.
23. 21Maher MA, Naha PC, Mukerjee SP, Byrne HJ. Numerical simulations of in vitro nanoparticle toxicity – the case of Poly(amido amine) dendrimers. Toxicol in Vitro. 2014;28:1449-60.
24. Nawaz H, Bonnier F, Knief P, Howe O, Lyng FM, Meade AD, Byrne HJ. Evaluation of the potential of Raman Microspectroscopy for prediction of chemotherapeutic response to cisplatin in lung adenocarcinoma. Analyst. 2010;135:3070-76.
25. Nawaz H, Bonnier F, Meade AD, Lyng FM, Byrne HJ. Comparison of subcellular responses for the evaluation and prediction of the chemotherapeutic response to cisplatin in lung adenocarcinoma using Raman spectroscopy. Analyst. 2011;136:2450-63.
26. Nawaz H, Garcia A, Meade AD, Lyng FM, Byrne HJ. Raman micro spectroscopy study of the interaction of vincristine with A549 cells supported by expression analysis of bcl-2 protein. Analyst. 2013;138:6177-84.
27. 22Poletto FS, Jager E, Cruz L, Pohlmann AR, Guterres SS. The effect of polymeric wall on the permeability of drug-loaded nanocapsules. Mat Sci Eng C. 2008;28:472-8.
28. 23Ravanello A, Dadalt G, Torres BGS, Hurtado FK, Marcolino AIP, Rolim CMB. Development and validation of an UV-spectrophotometric method for the dissolution studies of sitagliptin tablets. Latin Am J Pharm. 2010;29:962-7.
29. 24Atkinson KE. An Introduction to Numerical Analysis. 2nd ed. New York: John Wiley & Sons, Inc.; 1989.
30. 25Salvati A, Aberg C, Dos Santos T. Experimental and theoretical comparison of intracellular import of polymeric nanoparticles and small molecules: toward models of uptake kinetics. Nanomedicine: NBM. 2011;7:818-26.
31. 26Mukherjee SP, Byrne HJ. Polyamidoamine dendrimer nanoparticle cytotoxicity, oxidative stress, caspase activation and infammatory response: experimental observation and numerical simulation. Nanomedicine: NBM. 2013;9:202-11.
32. 27Kaufmann SH, Earnshaw WC. Induction of apoptosis by cancer chemotherapy. Exp Cell Res. 2000;256:42-9.

33. 28Black JW, Leff P. Operational models of pharmacological agonism. Proc R Soc Lond [Biol]. 1983;220:141-62.
34. 29Gewirtz DA. A critical evaluation of the mechanisms of action proposed for the antitumor effects of the anthracycline antibiotics adriamycin and daunorubicin. Biochem Pharmacol. 1999;57:727-41.
35. 30Nel A, Xia T, Mädler L, Li N. Toxic potential of materials at the nanolevel. Science 2006;311:622-7.
36. 31International Conference on Harmonisation (ICH). Validation of Analytical Procedures: Text and Methodology Q2(R1). 2005. http://www.ich.org/fileadmin/Public_Web_Site/ICH_Products/Guidelines/Quality/Q2_R1/Step4/Q2_R1__Guideline.pdf. Accessed 15 Jul 2015.
37. 32O'Brien J, Wilson I, Orton T, Pognan F. Investigation of the Alamar Blue (resazurin) fluorescent dye for the assessment of mammalian cell cytotoxicity. Eur J Biochem. 2000;267:5421-6.
38. 33De Fries R, Mitsuhashi M. Quantification of mitogen induced human lymphocyte proliferation: Comparison of alamarbluetm assay to 3h-thymidine incorporation assay. J Clin Lab Anal. 1995;9:89-95.
39. 34Poornima P, Kumar VB, Weng CF, Padma VV. Doxorubicin induced apoptosis was potentiated by neferine in human lung adenocarcinoma, A549 cells. Food Chem Toxicol. 2014;68:87-98.
40. 35Lv S, Tang Z, Li M, Lin J, Song W, Liu H, Huang Y, Zhang Y, Chen X. Co-delivery of doxorubicin and paclitaxel by PEG-polypeptide nanovehicle for the treatment of non-small cell lung cancer. Biomaterials. 2014;35:6118-29.
41. 36Farhane Z, Bonnier F, Casey A, Byrne HJ. Raman microspectroscopy for in vitro drug screening: subcellular localization and interactions of doxorubicin. Analyst. 2015;140:4212-23.
42. 37Prabaharan M, Grailer JJ, Pilla S, Steeber DA, Gong SQ. Amphiphilic multi-armblock copolymer conjugated with doxorubicin via pH-sensitive hydrazone bond for tumor-targeted drug delivery. Biomaterials. 2009;30:5757-66.
43. 38Li Q, Lv S, Tang Z, Liu M, Zhang D, Yang Y, Chen X. A co-delivery system based on paclitaxel grafted mPEG-b-PLG loaded with doxorubicin: Preparation, in vitro and in vivo evaluation. Int J Pharm. 2014;471:412-20.
44. 39Chittasupho C, Lirdprapamongkol K, Kewsuwan P, Sarisuta N. Targeted delivery of doxorubicin to A549 lung cancer cells by CXCR4 antagonist conjugated PLGA nanoparticles. Eur J Pharm Biopharm. 2014;88:529-38.

45. 40Wang X-B, Zhou H-Y. Molecularly targeted gemcitabine-loaded nanoparticulate system towards the treatment of EGFR overexpressing lung cancer. Biomed Pharmacother. 2015;70:123-8.
46. 41Uhrich KE, Cannizzaro SM, Langer RS, Shakesheff KM. Polymeric systems for controlled drug release. Chem Rev. 1999;99:3181-98.
47. Siddique MI, Katas H, Amin MCIM, Ng SF, Zulfakar MH, Buang F, Jamil A. Minimization of Local and Systemic Adverse Effects of Topical Glucocorticoids by Nanoencapsulation: *In Vivo* Safety of Hydrocortisone–Hydroxytyrosol Loaded Chitosan Nanoparticles. J Pharm Sci. 2015;104:4276-86.
48. Yoshitomita T, Ozakia Y, Thangavela S, Nagasakia Y. Redox nanoparticle therapeutics to cancer — increase in therapeutic effect of doxorubicin, suppressing its adverse effect. J Control Rel. 2013;172:137-43.

Tables

Table 1. Results of physicochemical characterisation of chitosan nanoparticles.

Parameter[a]	**CS-TPP**	**DOX-CS-TPP**
Number mean (nm)	509 ± 13	473 ± 41
Polydispersity index	0.28 ± 0.05	0.31 ± 0.2
Zeta potential (mV)	35 ± 4	34 ± 4
Particle concentration (particles/mL)	$3.7 \pm 0.2 \times 10^{12}$	$5.1 \pm 0.2 \times 10^{12}$

[a] Results are expressed as mean ± SD.

Figure Legends

Fig. 1 Experimental (symbols) and simulated (lines) exposure time and dose dependent viability, as measured using the MTT and Alamar Blue® (AB) assays, for A549 cells at 24, 48 and 72h. For (E) and (F) the x-axis label indicates the dose µM and particles per mL. Viability is expressed as the mean ± S.D. of the % decrease in formazan absorbance (for MTT) or resorufin fluorescence (for Alamar Blue®), as compared to the unexposed control of three independent experiments. (A) and (B) MTT and AB of CS-TPP; (C) and (D) MTT and AB of Free DOX; (E) and (F) MTT and AB of DOX-CS-TPP

Fig. 2 Fluorescence microscopy images of A549 cells after incubation with CS-TPP, free DOX or DOX-CS-TPP for 24h. The arrows highlight the co-localization of red fluorescence from DOX with blue nuclear stain (pinkish color) in Free DOX treated cells and predominantly less co-localization in DOX-CS-TPP treated cells

Fig. 3 Confocal microscopy images of A549 cells after incubation with CS-TPP, free DOX or DOX-CS-TPP for 4h. The arrows highlight the co-localization of DOX-CS-TPP with early endosomes (yellowish color)

Fig. 4 Simulated dose dependent cytotoxic responses for exposure to free DOX (A) MTT and (B) AB. (C) Simulated time dependent DOX uptake and cytotoxic responses of MTT and AB at a dose of 0.1 µM

Fig. 5 Simulated dose dependent cytotoxic responses for exposure to CS-TPP (A) MTT (B) AB. (C) Simulated time dependent CS-TPP nanoparticle uptake and cytotoxic responses of MTT and AB at a dose of 10^{10} particles/mL

Fig. 6 Simulated dose dependent cytotoxic responses for exposure to DOX-CS-TPP (A) MTT (B) AB. Simulated time dependent DOX-CS-TPP uptake and cytotoxic responses of (C) MTT and (D) AB at a dose of 10^{10} particles/mL (0.1µM of DOX)

Figure 1

A

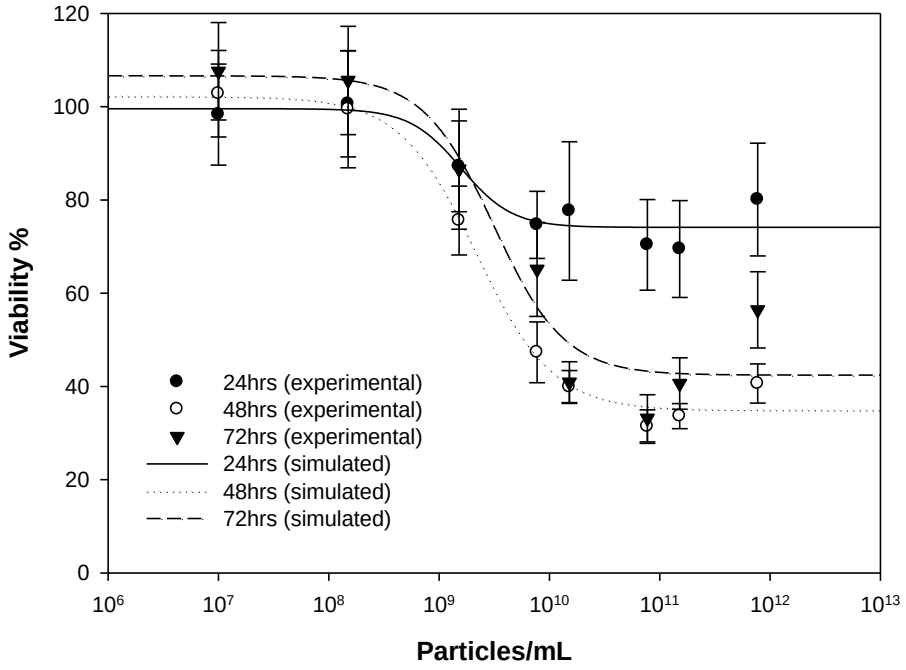
120
100
80
60
40
20
0
Viability %
24hrs (experimental)
48hrs (experimental)
72hrs (experimental)
24hrs (simulated)
48hrs (simulated)
72hrs (simulated)
10^6
10^7
10^8
10^9
10^10
10^11
10^12
10^13
Particles/mL

B

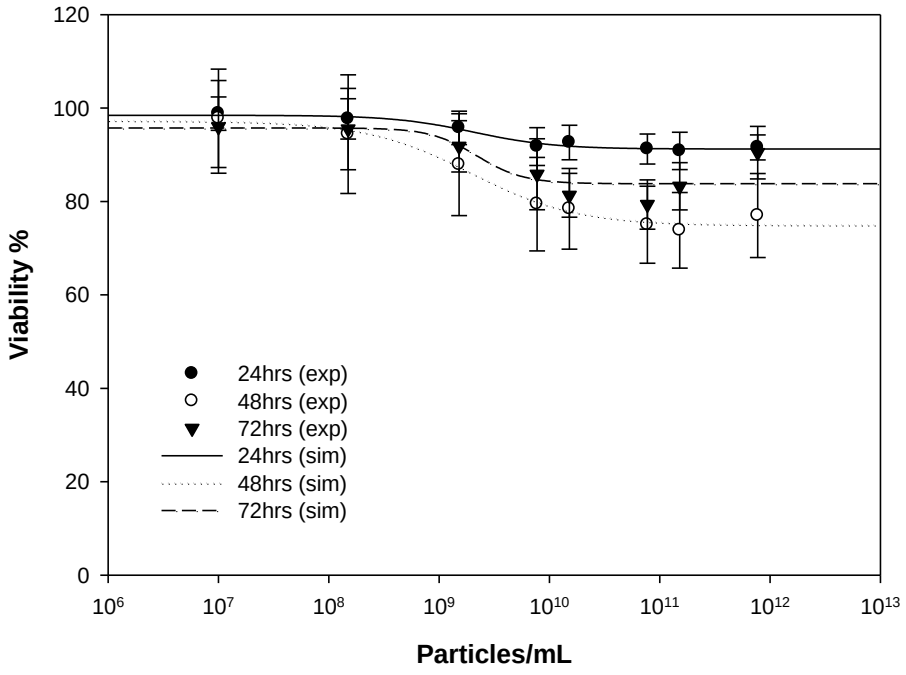
120
100
80
60
40
20
0
Viability %
24hrs (exp)
48hrs (exp)
72hrs (exp)
24hrs (sim)
48hrs (sim)
72hrs (sim)
10^6
10^7
10^8
10^9
10^10
10^11
10^12
10^13
Particles/mL

C

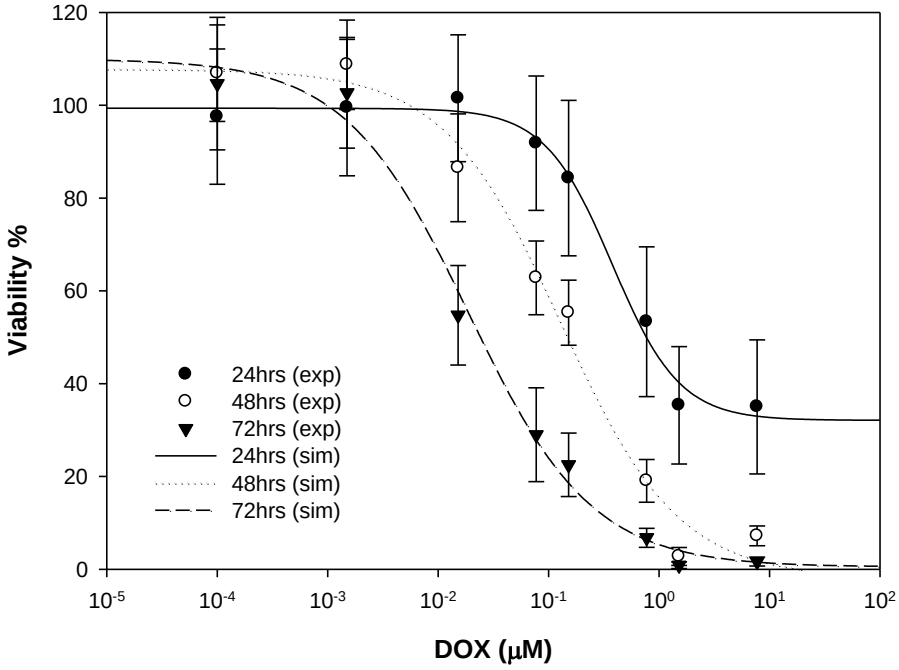
120
100
80
60
40
20
0
Viability %
24hrs (exp)
48hrs (exp)
72hrs (exp)
24hrs (sim)
48hrs (sim)
72hrs (sim)
10-5
10-4
10-3
10-2
10-1
100
101
102
DOX (μM)

D

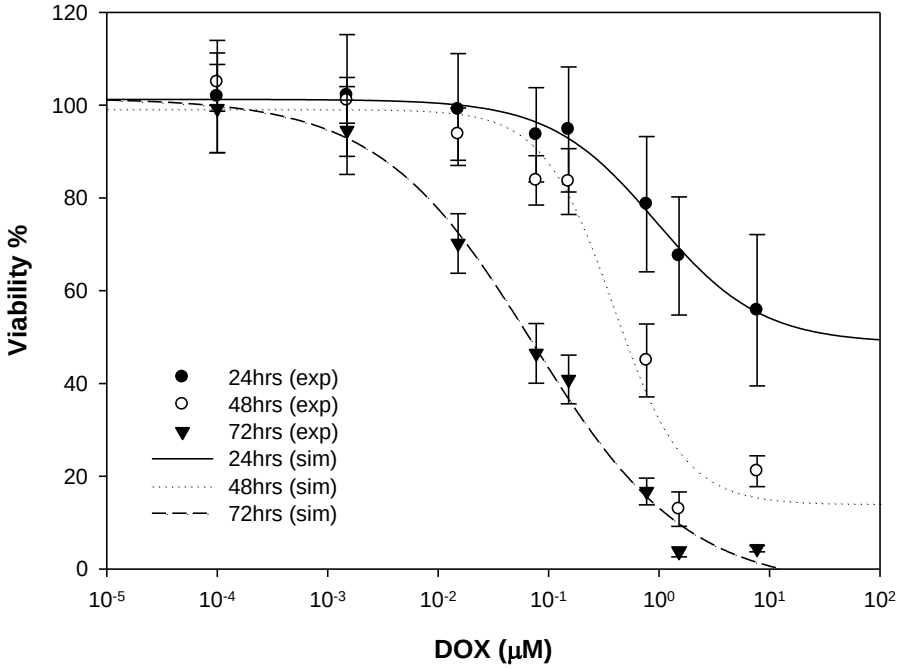
120
100
80
60
40
20
0
Viability %
24hrs (exp)
48hrs (exp)
72hrs (exp)
24hrs (sim)
48hrs (sim)
72hrs (sim)
10-5
10-4
10-3
10-2
10-1
100
101
102
DOX (μM)

E

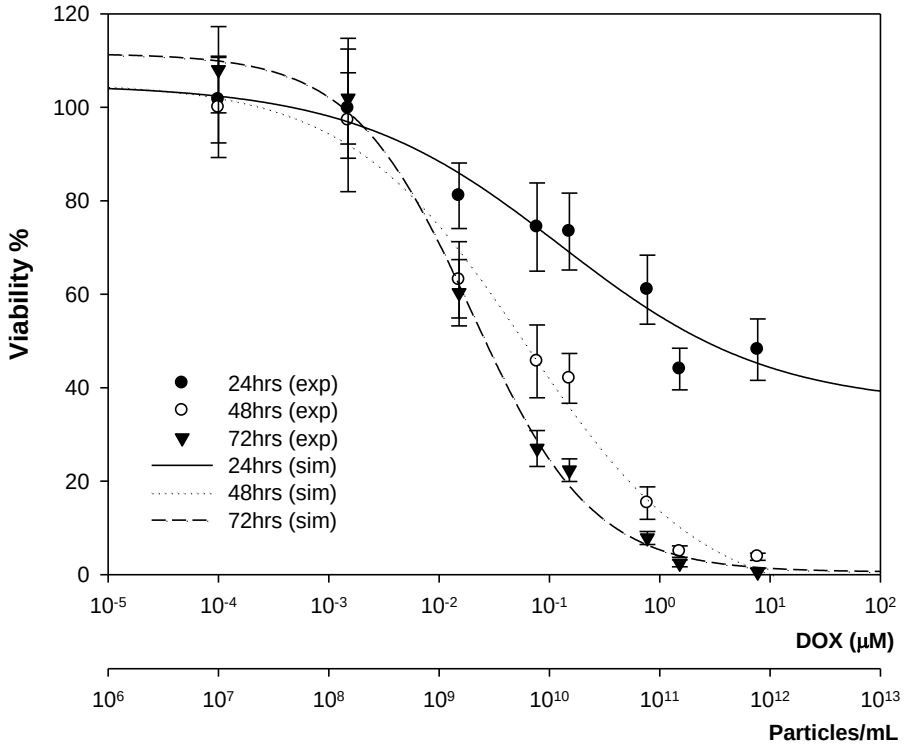
Viability %
120
100
80
60
40
20
0
24hrs (exp)
48hrs (exp)
72hrs (exp)
24hrs (sim)
48hrs (sim)
72hrs (sim)
10-5
10-4
10-3
10-2
10-1
100
101
102
DOX (µM)
106
107
108
109
1010
1011
1012
1013
Particles/mL

629

F

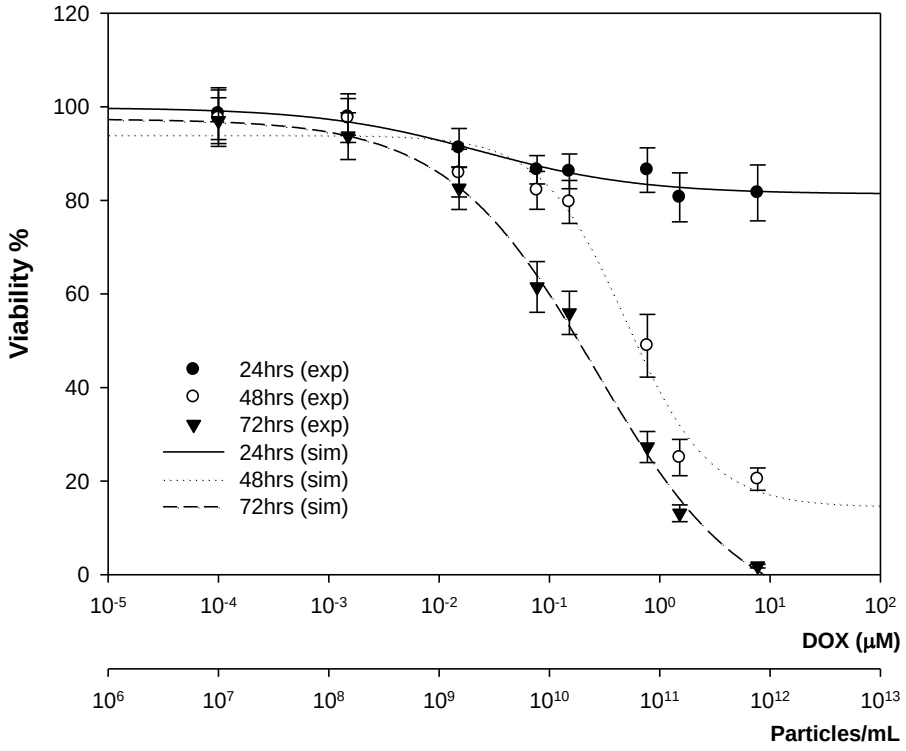
Viability %
120
100
80
60
40
20
0
24hrs (exp)
48hrs (exp)
72hrs (exp)
24hrs (sim)
48hrs (sim)
72hrs (sim)
10-5
10-4
10-3
10-2
10-1
100
101
102
DOX (µM)
106
107
108
109
1010
1011
1012
1013
Particles/mL

630

Figure 2

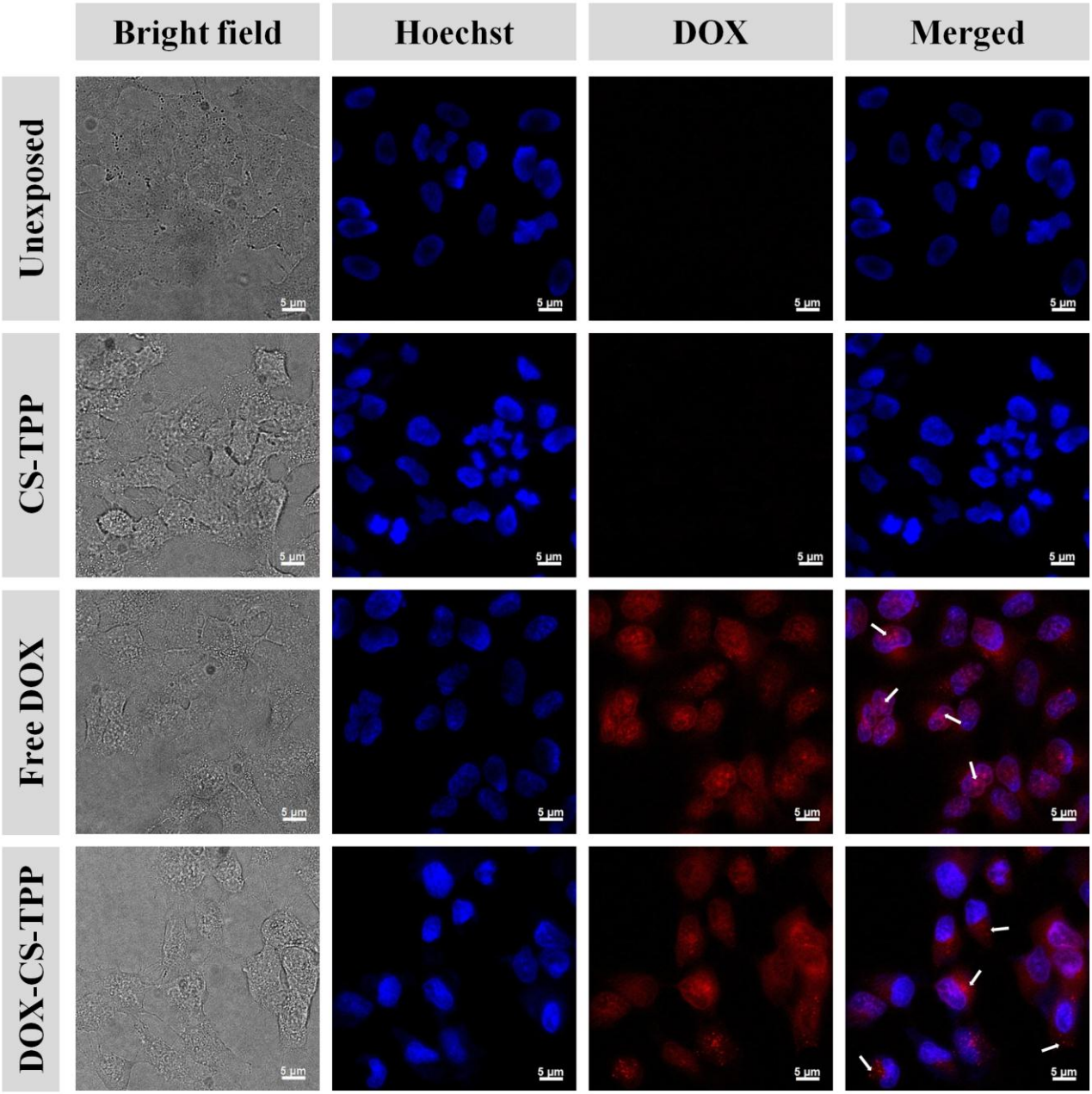
Bright field
Hoechst
DOX
Merged
Unexposed
CS-TPP
Free DOX
DOX-CS-TPP
5 µm

Figure 3

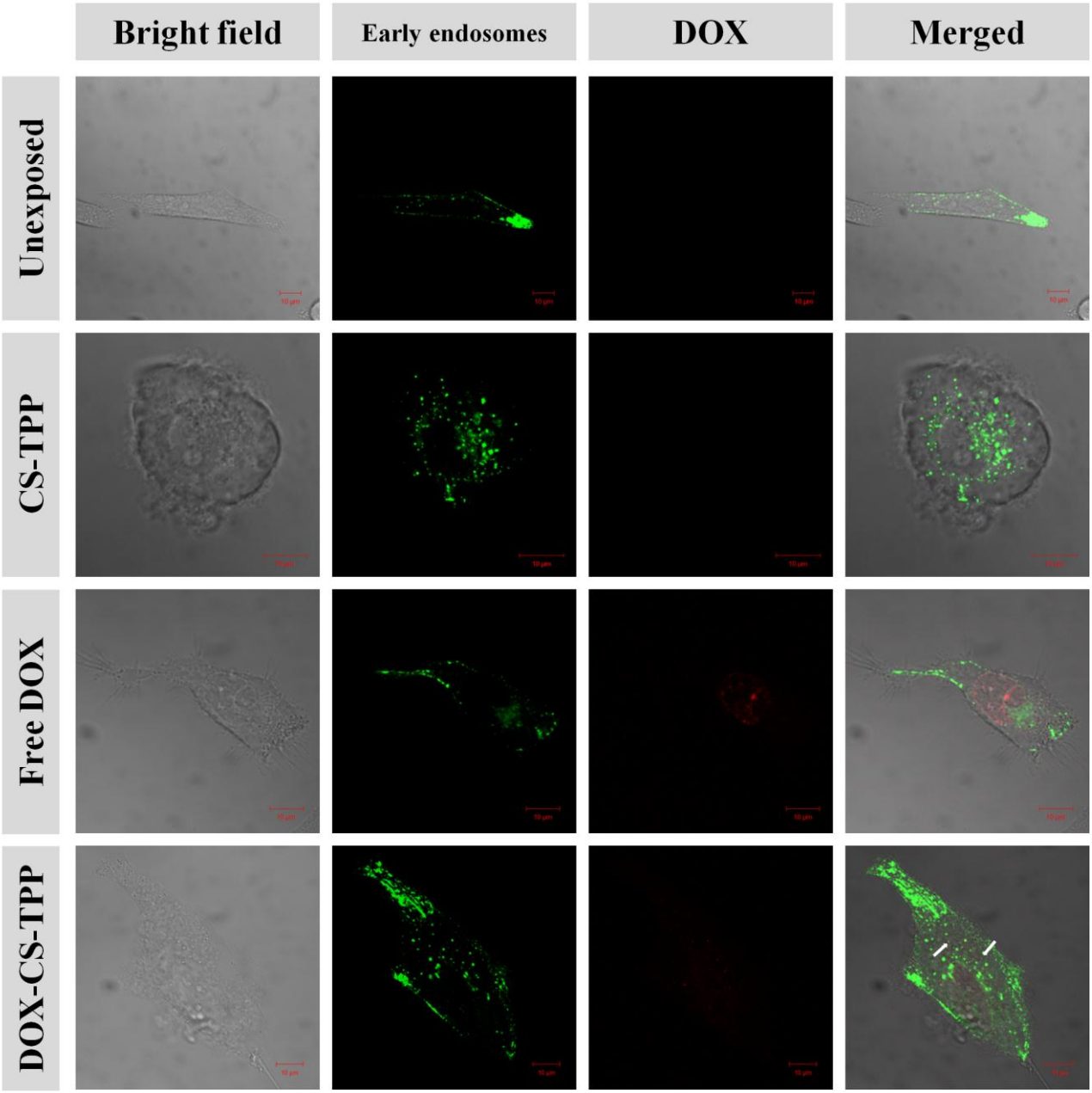
Bright field
Early endosomes
DOX
Merged
Unexposed
CS-TPP
Free DOX
DOX-CS-TPP

Figure 4

A

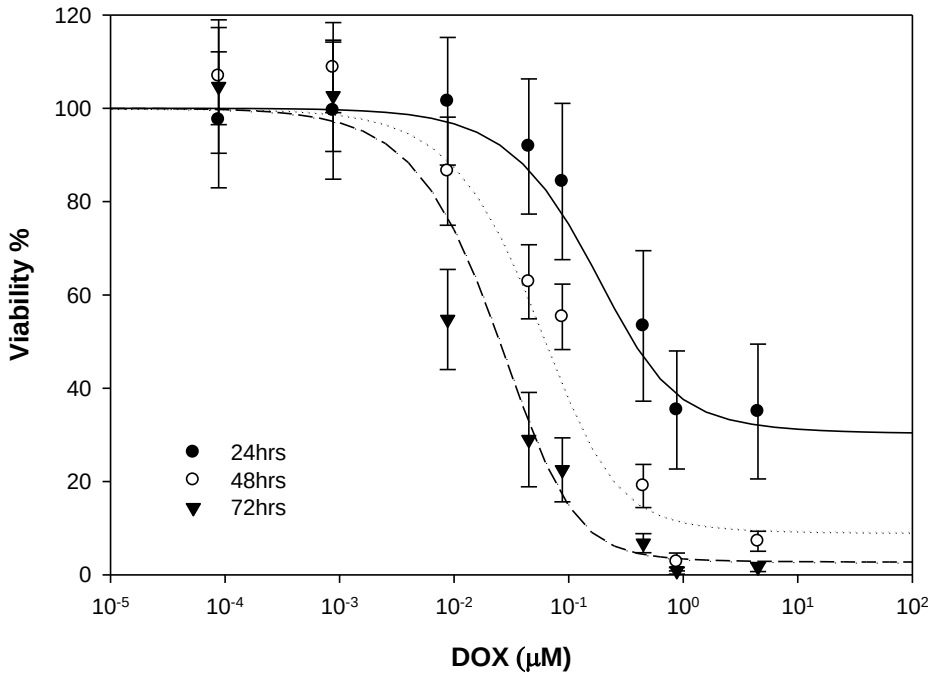
120
100
80
60
40
20
0
Viability %
24hrs
48hrs
72hrs
10-5
10-4
10-3
10-2
10-1
100
101
102
DOX (μM)

B

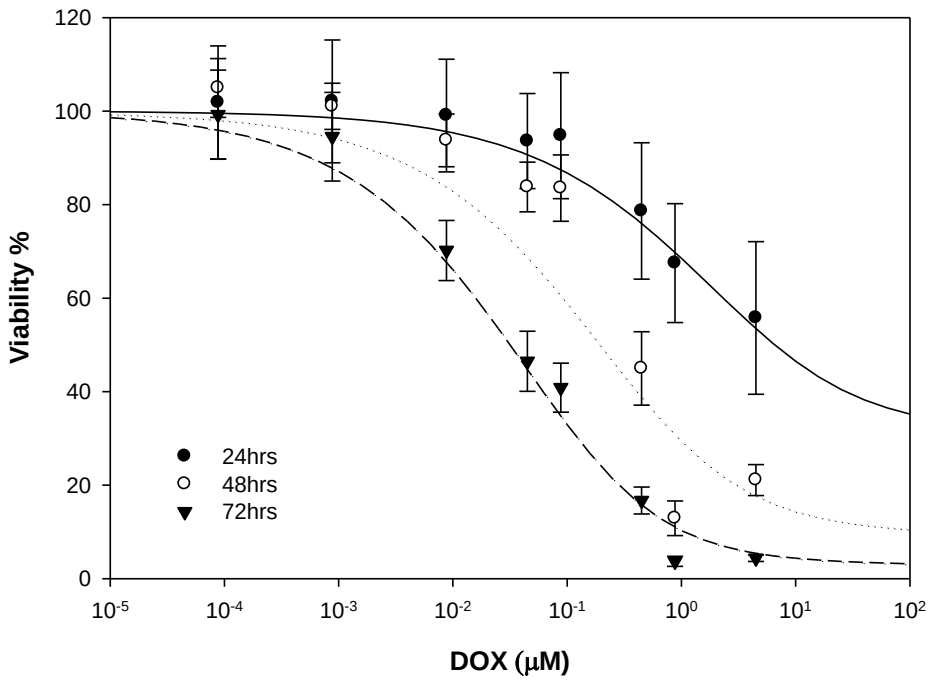
120
100
80
60
40
20
0
Viability %
24hrs
48hrs
72hrs
10-5
10-4
10-3
10-2
10-1
100
101
102
DOX (μM)

C

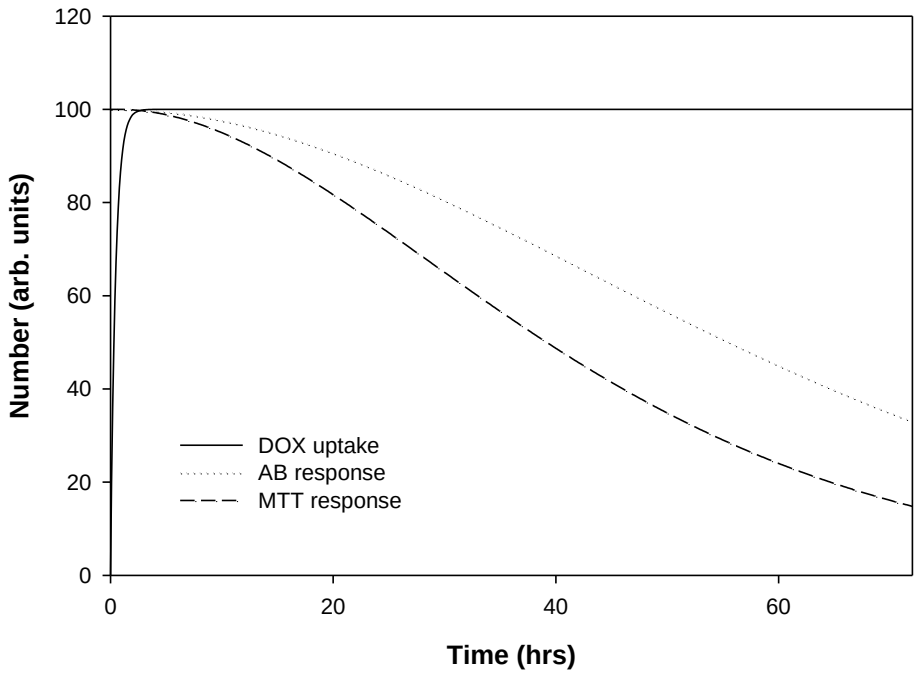
120
100
80
60
40
20
0
Number (arb. units)
0
20
40
60
Time (hrs)
DOX uptake
AB response
MTT response

Figure 5

A

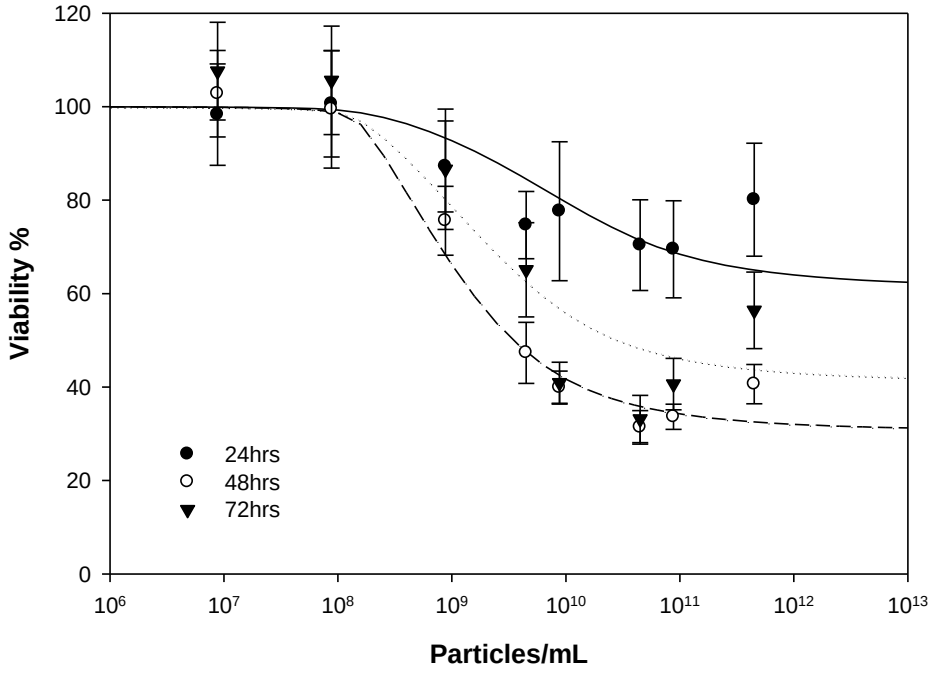
120
100
80
60
40
20
0
Viability %
24hrs
48hrs
72hrs
10^6
10^7
10^8
10^9
10^{10}
10^{11}
10^{12}
10^{13}
Particles/mL

B

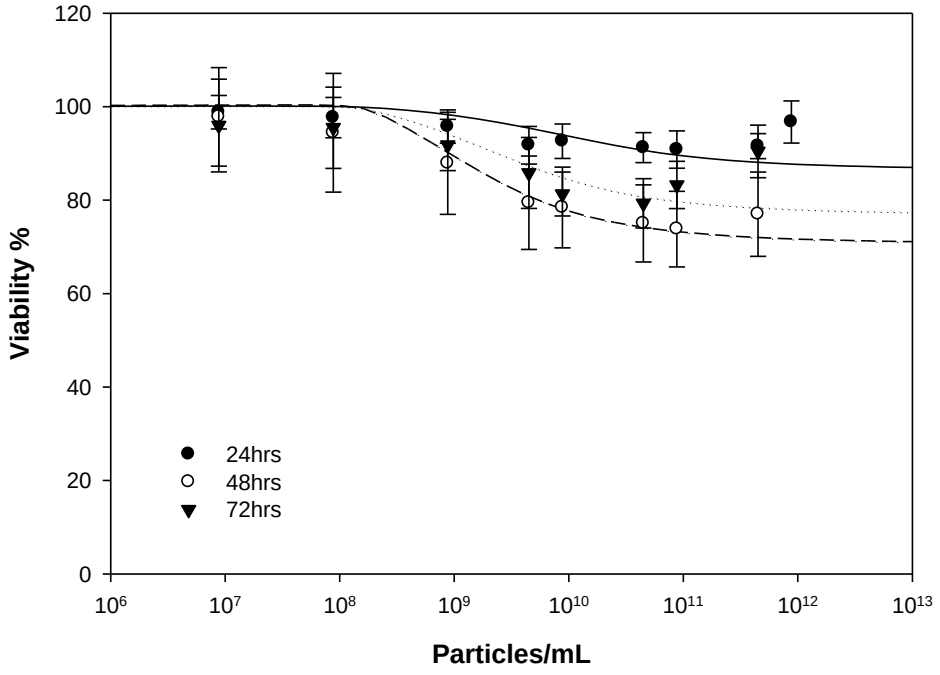
120
100
80
60
40
20
0
Viability %
24hrs
48hrs
72hrs
10^6
10^7
10^8
10^9
10^{10}
10^{11}
10^{12}
10^{13}
Particles/mL

C

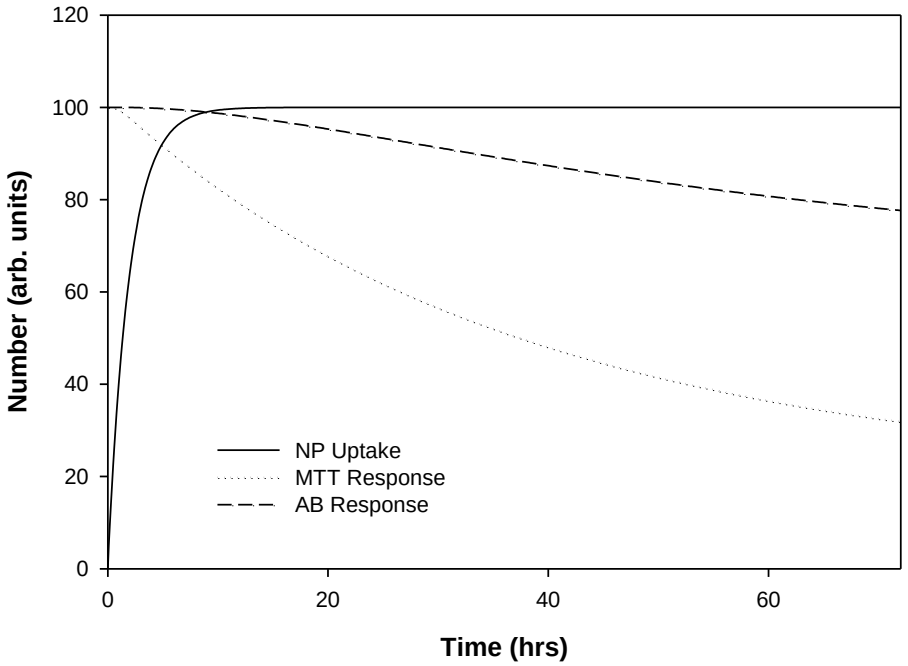
120
100
80
60
40
20
0
Number (arb. units)
0
20
40
60
Time (hrs)
NP Uptake
MTT Response
AB Response

Figure 6

A

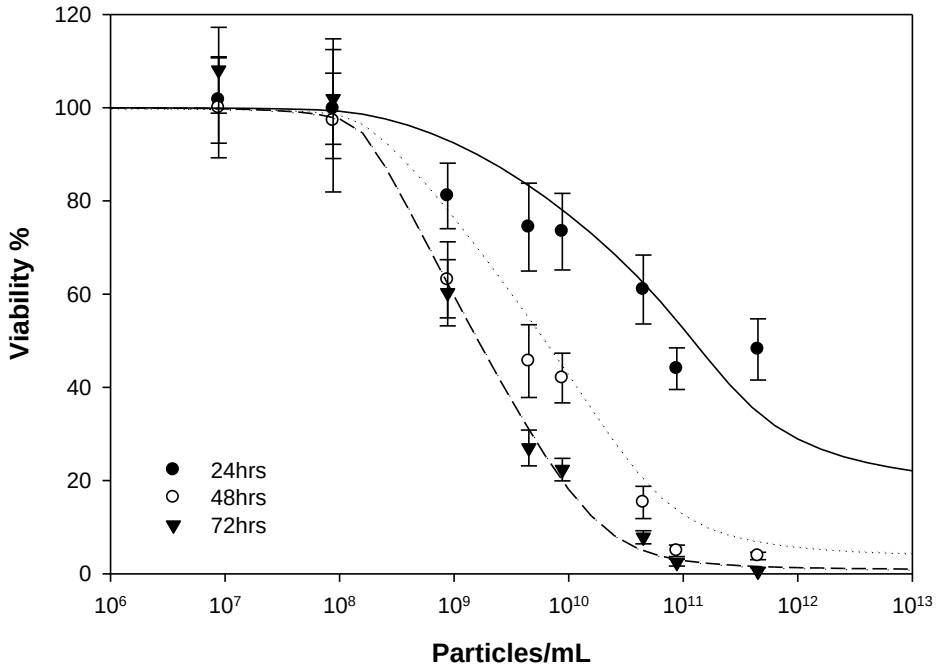
120
100
80
60
40
20
0
Viability %
24hrs
48hrs
72hrs
10⁶
10⁷
10⁸
10⁹
10¹⁰
10¹¹
10¹²
10¹³
Particles/mL

B

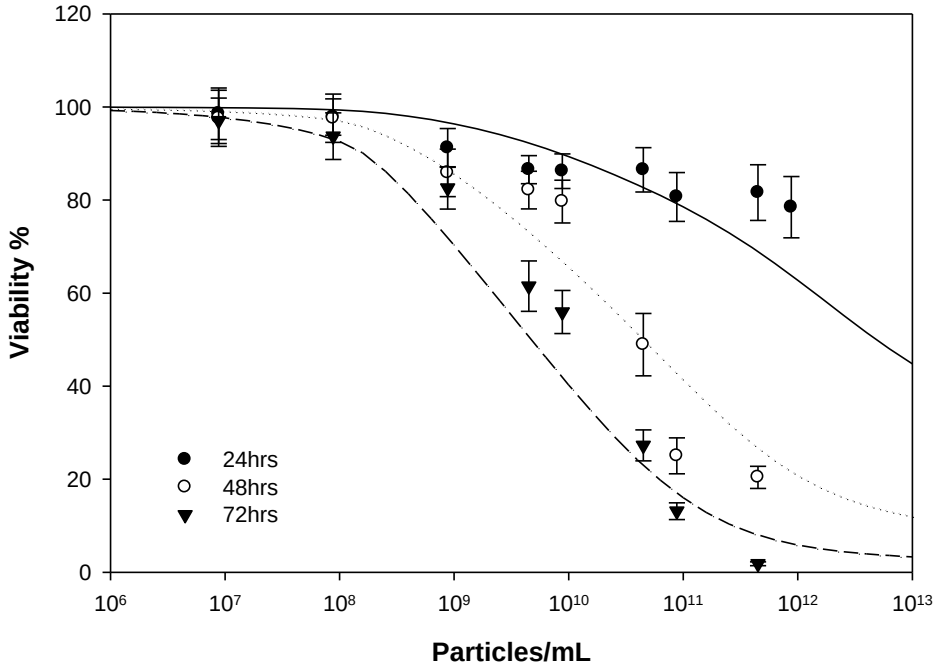
120
100
80
60
40
20
0
Viability %
24hrs
48hrs
72hrs
10⁶
10⁷
10⁸
10⁹
10¹⁰
10¹¹
10¹²
10¹³
Particles/mL

C

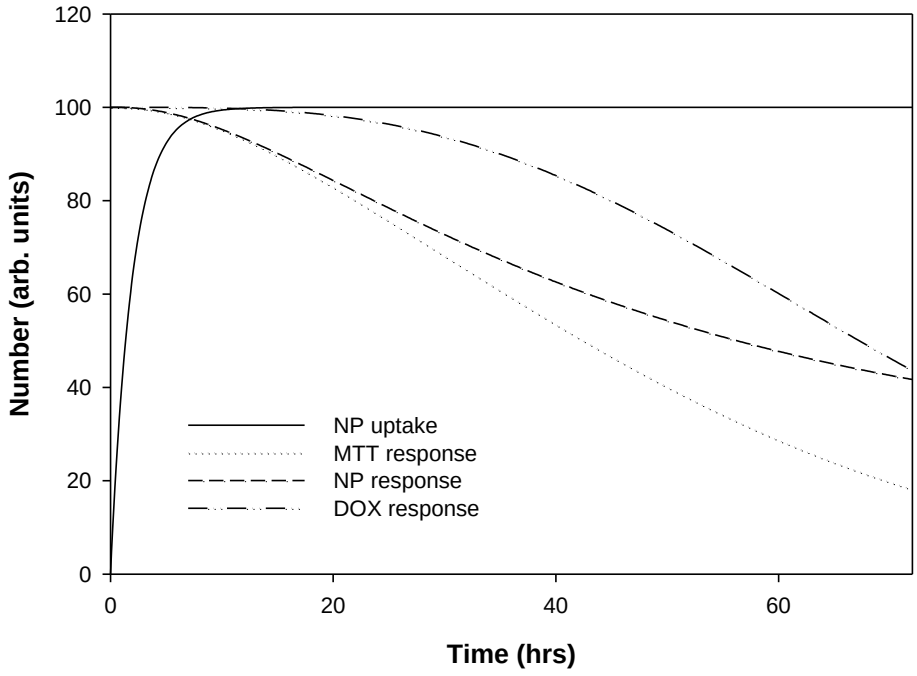
120
100
80
60
40
20
0
Number (arb. units)
0
20
40
60
Time (hrs)
NP uptake
MTT response
NP response
DOX response

D

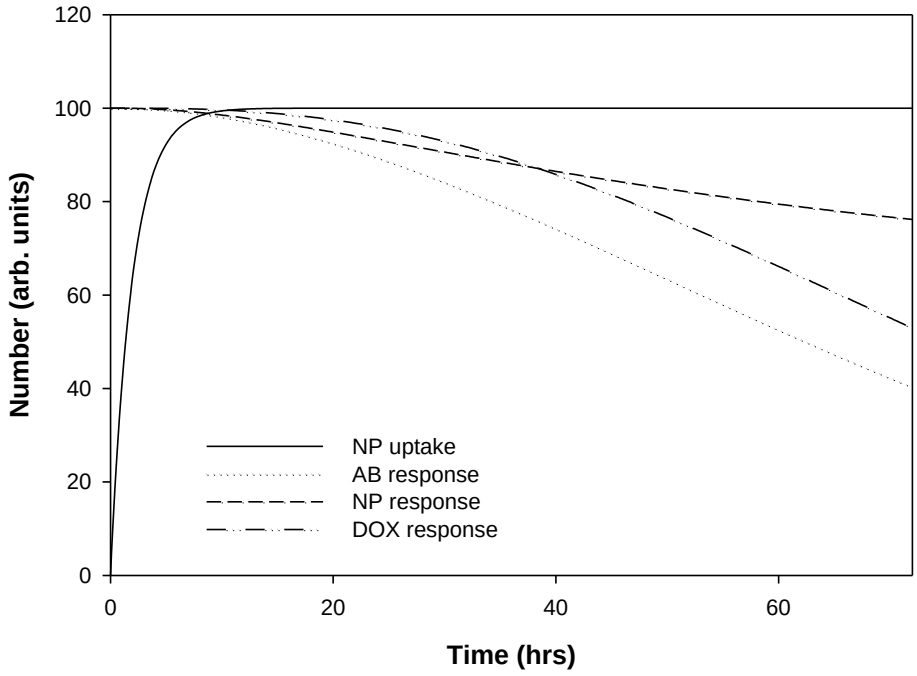
120
100
80
60
40
20
0
Number (arb. units)
0
20
40
60
Time (hrs)
NP uptake
AB response
NP response
DOX response